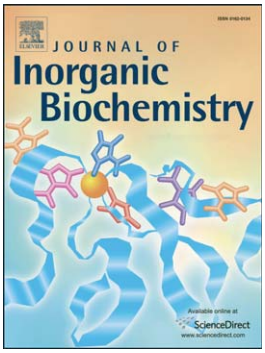

The key role of coligands in novel ruthenium(II)-cyclopentadienyl bipyridine derivatives: ranging from non-cytotoxic to highly cytotoxic compounds

Leonor Côrte-Real, M. Paula Robalo, Fernanda Marques, Guilherme Nogueira, Fernando Avecilla, Tiago J.L. Silva, Filipa C. Santos, A. Isabel Tomaz, M. Helena Garcia, Andreia Valente

PII: S0162-0134(15)30020-9
DOI: doi: 10.1016/j.jinorgbio.2015.06.015
Reference: JIB 9745

To appear in: *Journal of Inorganic Biochemistry*

Received date: 5 February 2015
Revised date: 15 June 2015
Accepted date: 15 June 2015

Please cite this article as: Leonor Côrte-Real, M. Paula Robalo, Fernanda Marques, Guilherme Nogueira, Fernando Avecilla, Tiago J.L. Silva, Filipa C. Santos, A. Isabel Tomaz, M. Helena Garcia, Andreia Valente, The key role of coligands in novel ruthenium(II)-cyclopentadienyl bipyridine derivatives: ranging from non-cytotoxic to highly cytotoxic compounds, *Journal of Inorganic Biochemistry* (2015), doi: 10.1016/j.jinorgbio.2015.06.015

The key role of coligands in novel ruthenium(II)-cyclopentadienyl bipyridine derivatives: ranging from non-cytotoxic to highly cytotoxic compounds

Leonor Côrte-Real,[a] *M. Paula Robalo,*[b,c] *Fernanda Marques,*[d] *Guilherme Nogueira,* [a] *Fernando Avecilla,*[e] *Tiago J. L. Silva,* [a] *Filipa C. Santos,* [a] *A. Isabel Tomaz,* [a] *M. Helena Garcia,***[a] *and Andreia Valente*[*,a]

[a]Centro de Química Estrutural, Faculdade de Ciências da Universidade de Lisboa, Campo Grande, 1749-016 Lisboa, Portugal.

[b]Área Departamental de Engenharia Química, Instituto Superior de Engenharia de Lisboa, Rua Conselheiro Emídio Navarro 1, 1959-007 Lisboa, Portugal.

[c]Centro de Química Estrutural, Instituto Superior Técnico, Universidade de Lisboa, Av. Rovisco Pais, 1049-001 Lisboa, Portugal.

[d]Centro de Ciências e Tecnologias Nucleares, Instituto Superior Técnico, Universidade de Lisboa, Estrada Nacional 10 (km 139.7) 2695-066 Bobadela LRS, Portugal.

[e]Departamento de Química Fundamental, Universidade da Coruña, Campus de A, Zapateria 15071, A Coruña, Spain.

[*] Corresponding author: Tel.: +351 217500898.

e-mail address: amvalente@fc.ul.pt (A. Valente).

[**] Corresponding author: Tel.: +351 217500088.

e-mail address: mhgarcia@fc.ul.pt (M.H. Garcia).

Abstract: A new family of eight ruthenium(II)-cyclopentadienyl bipyridine derivatives, bearing nitrogen, sulphur, phosphorous and carbonyl sigma bonded coligands, has been synthesized. Compounds bearing nitrogen bonded coligands were found to be instable in aqueous solution, while the others presented appropriate stabilities for the biologic assays and pursued for determination of IC_{50} values in ovarian (A2780) and breast (MCF7 and MDAMB231) human cancer cell lines. These studies were also carried out for the [**5**:HSA] and [**6**:HSA] adducts (HSA = Human Serum Albumin) and a better performance was found for the first case. Spectroscopic, electrochemical studies by cyclic voltammetry and Differential Functional Theory calculations allowed to get some understanding on the electronic flow directions within the molecules and to find a possible clue concerning the structural features of coligands that can activate bipyridyl ligands towards an increased cytotoxic effect. X-ray structure analysis of compound $[Ru(\eta^5\text{-}C_5H_5)(bipy)(PPh_3)][PF_6]$ (**7**; bipy = bipyridine) showed crystallization on C2/c space group with two enantiomers of the $[Ru(\eta^5\text{-}C_5H_5)(bipy)(PPh_3)]^+$ cation complex in the racemic crystal packing.

1. Introduction

Cancer claims the lives of millions of people worldwide every year. The high mortality inherent to cancer conditions together with the very debilitating side effects caused by the drugs in clinical use (mainly platinum-based drugs such as cisplatin) are self-explicative about the urgency to find new chemotherapeutic options. In this frame, ruthenium has been seen as a promising alternative metal due its unique chemistry in aqueous solution[1,2]. The two most well-known examples of this class of compounds, that entered Phase II clinical trials, are imidazolium *trans*-[tetrachloro(dimethyl sulfoxide)(1H-imidazole)ruthenate(III)] (NAMI-A)[3]

and indazolium trans-[tetrachlorobis(1H-indazole)ruthenate(III)] (KP1019)[4]. Though these two inorganic ruthenium(III) compounds present similar chemical structures, they exhibit completely different chemotherapeutic behaviour. While NAMI-A shows a marked efficiency against the formation of metastases[5], KP1019 has cytotoxic activity against a wide panel of human tumour models[4]. During the last decade other structurally different families of ruthenium compounds have been synthesized, some of them also exhibiting interesting potential. This is the case of the organometallic mononuclear piano-stool '$Ru^{II}(\eta^6\text{-}C_6H_6)$' complexes[6,7]. The literature concerning the isoelectronic '$Ru^{II}(\eta^5\text{-}C_5H_5)$' fragment has been less explored, although important results have been obtained combining this fragment with selective kinase inhibitors[8,9]. Our research group has been engaged in the synthesis of new ruthenium compounds based on the $[Ru^{II}(\eta^5\text{-}C_5H_5)(PP)(L)]^+$ structure (PP = monodentate or bidentate phosphane; L = monodentate or bidentate heteroaromatic ligand)[10 -16]. The results obtained for this family of compounds show cytotoxic activities in the nano- and sub-micromolar range against several human cancer cell lines (*e.g.* MiaPaCa, LoVo, PC3, HL-60, MCF7, HT29, A2780, A2780cisR) [10-16], placing them among the best cytotoxic Ru^{II}-arene complexes. In addition, these complexes present, in most cases, lower IC_{50} values than cisplatin. Factors that modulate the cytotoxic activity of Ru-based drugs are numerous, and seem to be dependent on the family compounds under scrutiny. We are interested in pinpointing/understanding whether (and how) structural factors control and potentiate the anti-tumour activity of ruthenium-cyclopentadienyl complexes. In this frame, the structure-activity performance of a new family of complexes of general formula $[Ru^{II}(\eta^5\text{-}C_5H_5)(bipy)(L)][PF_6]$ (bipy = 2,2'-bipyridine; L = imidazole (**1**), 1-benzyl-1-imidazole (**2**), 4-(1H-imidazol-1-yl)phenol (**3**), 1-(4-methoxyphenol)-1H-imidazole (**4**), dimethyl sulfoxide (**5**), carbon monoxide (**6**) and triphenylphosphane (**7**)) was designed using TM34, $[Ru^{II}(\eta^5\text{-}$

C_5H_5)(bipy)(PPh_3)][CF_3SO_3] [12], as a model. Thus, the introduction of coligand diversity was achieved by σ-coordination of different atoms, namely N, S, C and P. In addition, the precursor of these compounds, [Ru^{II}(η^5-C_5H_5)(bipy)($NCCH_3$)][PF_6] **8** was isolated and characterized for comparison and better understanding of the spectroscopic and electrochemical data.

2. RESULTS AND DISCUSSION

2.1. Synthesis of the Ru(II) complexes

Mononuclear complexes of the general formula [Ru(η^5-C_5H_5)(bipy)(L)][PF_6] with L = imidazole (**1**), 1-benzyl-1-imidazole (**2**), 4-(1H-imidazol-1-yl)phenol (**3**) and 1-(4-methoxyphenol)-1H-imidazole (**4**), were prepared, as shown in **Scheme 1**, by ligand substitution from the parent cationic complex [Ru(η^5-C_5H_5)(bipy)($NCCH_3$)][PF_6] **8** in dichloromethane, at room temperature, in the presence of a slight excess of the corresponding ligand. For complex **5**, [Ru(η^5-C_5H_5)(bipy)($NCCH_3$)][PF_6] was dissolved in *ca.* 200 µL of DMSO and 15 mL of water. After solvent removal, the complex was recovered as an orange compound. In the case of compound **6**, a flow of CO was passed through the solution for *ca.* 15 min, allowing the formation of the complex as an orange-brownish product. Compound **7** was synthesized by halide abstraction followed by ligand substitution from [Ru(η^5-C_5H_5)(PPh_3)$_2$Cl]. The new compounds were recrystallized by slow diffusion of *n*-hexane or diethyl ether in dichloromethane, acetonitrile or methanol solutions, giving crystalline orange to red compounds. All the compounds are fairly stable to air and moisture in the solid state and were obtained in good yields (50-90%).

The formulation and purity of all the new compounds is supported by analytical data, FT-IR spectroscopy, ^{1}H, ^{13}C, ^{31}P NMR spectroscopic data and elemental analyses. The solid state FT-

IR spectra (KBr pellets) of the complexes presented a large number of bands which identify the presence of the various fragments of the molecules. Characteristic bands were used to confirm the presence of the cyclopentadienyl (*ca.* 3140-3000 cm^{-1}), the bipyridine ligand (*ca.* 1520-1400 cm^{-1}) and the PF_6^- anion (≈ 840 and 560 cm^{-1}) in all the studied complexes. The infrared spectrum of compound **5** confirms the coordination of DMSO ligand through the sulphur atom due to the presence of a band at 1094 cm^{-1} attributed to $\nu_{S=O}$ and the absence of any significant vibration in the 920-930 cm^{-1} range, characteristic of coordination by the oxygen atom. It has been reported in the literature that in ruthenium complexes, a sulphur–bounded DMSO exhibits a distinctive $\nu_{S=O}$ band between 1080 and 1150 cm^{-1}, depending on the electronic nature of the other ligands in the coordination sphere, while an oxygen-bounded form shows a signal of slightly lower energy between 900 and 1000 cm^{-1} [17-20]. The positive shift in the $\nu_{S=O}$ of *ca.* 44 cm^{-1} can be explained by the inversed polarization of the sulfoxide π-bond effect [21]. Also, in the case of compound **6**, the coordination of carbon monoxide can be confirmed by the infrared stretching vibration occurring at 1970 cm^{-1}. Besides, the observed shift of *ca.* -200 cm^{-1} in the $\nu_{C\equiv O}$ is indicative of a strong π-backdonation effect ($\nu_{C\equiv O,\ gas}$ = 2143 cm^{-1} [23] *vs.* $\nu_{C\equiv O}$ = 1970 cm^{-1} in compound **6**) which was further corroborated by our ^1H NMR studies (see below).

Scheme 1.

Analysis of the overall ^1H NMR results presented on **Table S1** showed that, comparing with $[Ru(\eta^5\text{-}C_5H_5)(NCMe)_3][PF_6]$, the substitution of the acetonitrile ligands by bipyridine and L ligands leads to a general deshielding on $\eta^5\text{-}C_5H_5$ protons, which extension is related with the π-acceptor capability of the L coligands. For compounds **1**-**4** the cyclopentadienyl ring displayed

signals in the characteristic range of monocationic ruthenium(II) (≈ 4.5 ppm). In the case of compounds **5**-**7** a marked deshielding of 0.6-1.2 ppm on these protons was observed, especially in the case of compound **6**, presenting the CO coligand. This observation clearly corroborates the π-backdonation effect found in our FT-IR studies. The chemical shifts observed for the protons of coordinated bipyridine on compounds **1**-**6** are very close of the uncoordinated ligand ones revealing that the deshielding expected upon a dative σ coordination of bipyridine ligand is compensated by the shielding due to π-back electronic flow towards the bipyridyl coordinated molecule (**Table S1**). Surprisingly compound **7** revealed a shielding of 0.33 ppm on the bipyridyl *ortho* protons. This observation might be explained by the effect of one of the phenyl ring current on the *ortho* bipy ligand, which adequate orientation and close proximity can be observed on the ORTEP plot for the cation complex $[Ru(\eta^5\text{-}C_5H_5)(bipy)PPh_3]^+$ (see below). Relatively to the effect observed on the coordination of the coligands, complexes **1**-**4**, showed a shielding of ~0.5 ppm on the H_4 proton of the coordinated imidazole ring in all cases, while the remaining protons are almost unchanged. This electronic density at the imidazole ligands also suggests the existence of some π-backdonation effect to this coligand. For complex **5** (bearing the *S*-bound DMSO coligand), a downfield shift of ^1H and ^{13}C resonances for the methyl groups upon coordination is consistent with the sulfur coordination mode[19] and corroborates the obtained FT-IR results. Globally it is observed that $\eta^5\text{-}C_5H_5$ ring releases the electronic flow through the ruthenium centre toward coligands and bipyridyl ligand. Thus, a general trend on this electronic flow towards the L coligand was observed for compounds **1**-**6** being this effect stronger in the case of CO. The additional electronic effect originated by PPh_3 on compound **7** leads to an asymmetric charge distribution on the N-heteroaromatic bipyridyl ligand, and consequently an important shielding on the bipyridyl *ortho* protons is observed.

2.2. UV-visible (UV-Vis) studies

Optical absorption spectra of these new seven [Ru(η^5-C_5H_5)(bipy)(L)][PF_6] complexes together with all ligands were recorded in 10^{-6} – 10^{-3} M dichloromethane solutions (see Experimental Section). **Figure 1a** shows the spectrum of compound **1** in dichloromethane and typifies the general behaviour of all the compounds. All the studied complexes showed two intense bands in the UV region attributed to π – π* electronic transitions occurring in the aromatic rings and a quite complex pattern occurring in the visible region (400-600 nm) with $\varepsilon_{max} \sim 5x10^3$ $M^{-1}cm^{-1}$ that can be related to several metal to ligand charge transfer bands (MLCT), from Ru 4d to π* N-heteroaromatic rings for compounds **1**-**4**. This pattern was also observed for compounds **5**-**7** and it is also compatible with the occurring MLCT effect originated by DMSO and CO coligands. In order to infer about the charge transfer character of these bands, further electronic spectra were obtained in acetonitrile and DMSO (see experimental section). Although no significant solvatochromic effect had been observed within the used polarity solvent range, an elucidation on the complexity on the lower energy band was noticeably found. To get some understanding about the influence of the several coligands presenting quite different donor-acceptor abilities (N-heteroaromatic derivatives, CO, DMSO and PPh_3) a detailed comparison was carried out to infer about the shift of these MLCT bands (**Figure 1b**). Compounds **1**-**4** containing N-heteroaromatic coligands presented MLCT bands occurring at the lowest energy. In **Figure 1b** one can compare the behaviour of compounds **1** , **5** and **7** (with medium π acceptor coligand) and **6** (with the best π acceptor coligand). The shifts observed on the energy of the MLCT band seem to be related with the π-backdonation from Ru to the coligand L (in accordance with Cp chemical

shifts).Thus, compounds presenting the highest π-backdonation present the lowest energy MLCT band (**1**-**4** < **7** < **5** < **6**).

Figure 1.

The newly synthesized complexes are soluble in dichloromethane, acetonitrile, acetone and DMSO. Their solubility in water/aqueous media is low to moderate, but this drawback is easily overcome by adding a low amount of DMSO as a co-solvent.

Envisaging the use of these new compounds as cytotoxic agents and their study in human cancer cell lines, their stability and behaviour in aqueous solution was studied in HEPES buffer at pH 7.4, using 2-3% DMSO, by UV-Vis spectroscopy. For compounds **1**-**4**, one can readily observe an immediate colour change once the solution is prepared: firstly the compounds were dissolved in DMSO and when upon dilution in water or aqueous buffered medium they changed from their original colour (orange or red) to yellow. This transformation in compound **2** was somehow slower and it was monitored by UV-Vis spectroscopy. As showed in **Figure S1a**, the MLCT band occurring at ~ 455 cm^{-1} completely vanishes after 45 minutes. Moreover, the electronic spectrum of this solution was found superposed with the one of compound **5** showing the substitution of the imidazole ring by DMSO (**Figure S1b**). Due to instability of complexes **1**-**4** in DMSO/water system, our *in vitro* biological studies were only carried on using compounds **5**-**7**, which were found to present adequate stability. Compound **7** showed some precipitation after *ca.* 4 h at concentrations suitable for UV-Vis spectroscopy; however, when working at lower concentrations (*e.g.* fluorescence studies and cellular viability studies), no precipitation was observed.

2.3. Single crystal structure of [Ru(η^5-C_5H_5)(PPh_3)(bipy)][PF_6] 7

[Ru(η^5-C_5H_5)(bipy)(PPh_3)][PF_6]·$(CH_3)_2CO$ **7** crystallized from acetone-d_6 solution (used for the NMR studies) as orange prisms (crystal dimensions 0.56 x 0.34 x 0.23 mm). **Figure 2** shows an ORTEP representation of [Ru(η^5-C_5H_5)(bipy)(PPh_3)]$^+$ cation **7.**

Figure 2.

The asymmetric unit contains one cationic ruthenium complex, one PF_6^- anion and one acetone molecule. In the molecular structure, the ruthenium centre adopts the expected "piano stool" distribution formed by the ruthenium-Cp unit bound to the nitrogen atoms of the bipy ligand. One phosphane group occupies the remaining coordination position. The distance for Ru-P bond is Ru(1)-P(1) = 2.3021(5) Å, and distances for Ru-N bonds are Ru(1)-N(1) 2.0731(14) Å and Ru(1)-N(2) 2.0712(14) Å. The distance between Ru and the centroid of the π-bonded cyclopentadienyl moiety is 1.821 Å to Ru centre (ring slippage 0.045 Å). The mean value of the Ru-C bond distance is 2.1848(18) Å. **Table S2** contains selected bond lengths and angles for compound **7**. π-π stacking interactions are absent in the structure since the distance between the bipyridine ligand ring N(1)-C(24)-C(25)-C(26)-C(27)-C(28) and the phosphane phenyl ring C(12)-C(13)-C(14)-C(15)-C(16)-C(17) is 4.140 Å. Contrarily, for the reported structure of cation complex [Ru(η^5-C_5H_5)(bipy)(PPh_3)]$^+$[CF_3SO_3]$^-$,[12] π-π stacking interactions can be observed. In addition, X-ray structure of **7** shows two enantiomers for the cation complex [Ru(η^5-C_5H_5)(bipy)PPh_3]$^+$ in the racemic crystal (space group C2/c). The chirality is due to a twist of the PPh_3 and Cp units. The cation complex [Ru(η^5-C_5H_5)(bipy)(PPh_3)]$^+$ presents a mirror plane

which contain P, Ru and the centroid of Cp ring (see **Figure S2**)[25]. The two enantiomers present in the $[Ru(\eta^5\text{-}C_5H_5)(bipy)PPh_3]^+$ crystal are herein reported for the first time.

2.4. Electrochemical experiments

The electrochemical behaviour of this family of ruthenium complexes $[Ru(\eta^5\text{-}C_5H_5)(bipy)(L)][PF_6]$ was studied by cyclic voltammetry in dichloromethane and in acetonitrile solutions containing ammonium hexafluorophosphate as supporting electrolyte (**Table S3** and **Table S4**, see supplementary information).

No redox processes for the free ligands were observed in dichloromethane, with exception of 1-(4-methoxyphenyl)-1H-imidazole (1-MPI, L for complex **4**), which showed a reductive process at E_{pc} = -0.84V. The cyclic voltammogram of complex $[Ru(\eta^5\text{-}C_5H_5)(bipy)(4\text{-IMP})]^+$ **3** (4-IMP = 4-(1H-imidazol-1-yl)phenol) (**Figure 3**) is representative of the general behaviour of this family in dichloromethane. All the complexes showed one quasi-reversible redox process at positive potentials, attributed to the Ru(II)/Ru(III) redox pair, with a lower intensity for the cathodic wave when compared with the anodic current. Nevertheless, when the scan rate direction is reversed immediately after the oxidation potential this decrease is less pronounced; this might indicate that the ruthenium oxidation is followed by a chemical reaction leading to non reductible species. For complexes **2** and **5**, an irreversible reductive process at negative potentials (E_{pc} = -1.13 and -1.26 V, respectively) was observed and attributed to a ligand-based reductive process.

The effect of the different coligands in the electronic environment of the ruthenium centre was assessed by comparison of the oxidation potentials for complexes **1**-**4** with complexes **5** and **7**, bearing the dimethyl sulfoxide and triphenylphosphane ligands respectively, instead of an imidazole derivative. In general, the presence of the monodentate imidazole based ligand lowered the oxidation potential of ruthenium centre, up to 500 mV. However, the substitution in

the imidazole ring did not lead to a substantial change on the electronic environment of the metal centre, since the Ru(II)/Ru(III) potential remained almost unchanged ($E_{1/2}$ ~ 0.65 to 0.68 V). Finally, for complex [Ru(η^5-C_5H_5)(bipy)(CO)][PF_6] **6**, the absence of any redox processes at the positive potentials range is in agreement with our spectroscopic data. The strong π-backdonation effect pulls the electronic density from the ruthenium center to CO coligand, shifting the ruthenium oxidation process out of the solvent potential window. In accordance, a quasi-reversible redox process within the bipyridine ligand was observed at $E_{1/2}$ = -1.32 V.

Figure 3.

Concerning the electrochemical behaviour in acetonitrile, for the imidazole-based ligands (1-benzyl-1-imidazole (1-BI), 4-(1H-imidazol-1-yl)phenol) (4-IMP)) and 2,2'-bipyridine no redox processes were observed. Imidazole (ImH) and 1-(4-methoxyphenyl)-1H-imidazole (1-MPI) showed two irreversible processes each one.

For the ruthenium(II) complexes, the behaviour is much more complicated leading generally to several undefined redox processes (some of them less intense than the one attributed to the metal centre), which indicates that the complexes are less stable in this solvent. In general, all the complexes exhibited one irreversible or quasi-reversible oxidation process at the positive potentials, attributed to the Ru(II)/Ru(III) redox pair (**Figure 4**) with a less intense cathodic wave, in accordance with the previous behaviour in dichloromethane. At the negative potential range, complexes **1**-**4** display one or two irreversible reductive processes which can be attributed to reductions within the N-heteroaromatic coligands. For complexes **5**-**8**, the irreversible (**5** and

8) or quasi-reversible (**6** and **7**) reductive processes found around -1.40 V, can be assigned to the bipy ligand.

The lability observed for the heteroaromatic ligands during the stability studies (see **Figure S1**) make us consider the possible replacement of these ligands by the acetonitrile coordinative solvent during the electrochemical experiments. Thus, the electrochemical behaviour of the parent compound $[Ru(\eta^5\text{-}C_5H_5)(NCMe)_3][PF_6]$ and the precursor $[Ru(\eta^5\text{-}C_5H_5)(bipy)(NCMe)][PF_6]$ (**8**), (which was isolated and characterized for this purpose, see Experimental Section) was also studied in the same experimental conditions. Comparison of the cyclic voltammograms of complexes **1** and **3** with $[Ru(\eta^5\text{-}C_5H_5)(NCMe)_3][PF_6]$ showed that substitution of all ligands by acetonitrile solvent molecules did not occur. Nevertheless, comparison with $[Ru(\eta^5\text{-}C_5H_5)(bipy)(NCMe)][PF_6]$ **8** showed that the second oxidative process is due to the formation of these latter species by replacement of the N-heteroaromatic coligand by one acetonitrile molecule (**Figure 4**). Complex $[Ru(\eta^5\text{-}C_5H_5)(bipy)(CO)][PF_6]$ **6** did not show any oxidation process in the solvent window compatible with its redox behaviour in dichloromethane.

Our electrochemical results showed that substitution of the imidazole based ligands by DMSO, CO, acetonitrile or PPh_3 provides an increase on the oxidation potential of the ruthenium centre. **Figure 5** compares the oxidation potentials of Ru(II)/Ru(III) pair and shows the trend ability of the ruthenium centre for oxidation: ImH ~ 1-BI > 4-IMP ~ 1-MPI > $NCCH_3$ > DMSO > PPh_3 >>CO. This trend revealed the net electronic density at the ruthenium centre which is a result of the different σ and π ability of the ligands. Therefore compounds possessing the most demanding coligands (CO, PPh_3 and DMSO) present the highest redox oxidation potentials.

Figure 4.

Figure 5.

2.5. Density Functional Theory (DFT) Studies

In order to further support our spectroscopic data we performed DFT calculations in cationic complexes **1** and **5**-**7**. The optimized structures are shown in **Figure S3** and the relevant structural parameters are shown in **Table 1**. Comparison of the crystallographic data of **7** with its DFT optimized structure showed a good agreement in the Ru-Cp and Ru-N bond distances, with differences of only +0.08 Å and +0.05 Å, respectively. DFT calculations predicted a slightly longer Ru-P bond distance, where a difference of +0.17 Å was observed. This value is however in the same range found for other CpRu related complexes[24]. Hence, it is fair to state that the rather modest 6-31G(d,p)/M06L-DFT level of theory is adequate to compute the geometries of this family of complexes.

Table 1.

π-backdonations from the organometallic fragment to the Cp, L and bipy ligands were assessed by charge decomposition analysis (CDA) and are also showed in **Table 1.** Noteworthy is the fact that both the triphenylphosphane and CO ligands in complexes **7** and **6**, respectively, originate relatively high estimated π-backdonations to the corresponding coligands L, proving the enhanced stability of these two compounds. π-backdonations to the bipy fragment ($[CpRuL]^{+}\rightarrow$bipy) were estimated in 0.543, 0.658, 0.598 and 0.584 electrons for **1**, **5**, **6** and **7**, respectively, showing that DMSO ligand (poor π-acceptor) leads to the highest π-backdonation

to the bipy fragment. Nevertheless this effect is not so noticeable in the proton NMR chemical shifts of the coordinated bipy.

The electronic spectra of the molecules were computed under the Time-dependent density functional theory (TD-DFT) formalism, with the inclusion of solvation effects by the PCM model. Acetonitrile was the solvent chosen for these studies. As an example, the TD-DFT spectrum of compound **7**, alongside with its experimental spectrum in acetonitrile, are depicted in **Figure 6.** In **Table 2** are selected main vertical optical transitions that contribute to the overall calculated spectrum.

Figure 6.

Our TD-DFT results confirmed the overall behaviour of the complexes, where an intense UV band was obtained, together with several low intensity bands in the visible region. The estimated wavelength of the UV absorption band is very close to the experimental value (λ_{exp} = 290 nm; λ_{calc} = 281 nm). An analysis of the molecular orbitals involved allowed the attribution of this band to a combination of a $\pi_{phosphane}$ - π^*_{bipy} transition (inter ligand transition) with a $d_{Ru} - \pi^*_{bipy}$ transition (MLCT). The overall shape of the spectra in the visible region is similar to the calculated spectra. The calculated maxima of absorption of the three visible bands are also in good agreement with the experimental maxima absorption, for which differences of only 3, 9 and 3 nm were obtained when going from the highest to the lowest energy transitions (**Table 2**), respectively. These bands were all attributed to MLCT charge transfers, $d_{Ru} - \pi^*_{bipy}$ transitions, together with $d_{Ru} - \pi^*_{phosphane}$ transitions. In fact, it is not uncommon that UV-Vis bands of organometallic complexes cover several transitions. This is the case of the present complex

where the calculated transition at 356 nm comprises four vertical excitations, as can be seen in **Table 2**.

Table 2.

2.6. Biologic Studies

2.6.1. In vitro cytotoxicity

The cytotoxic activity of compounds **5**-**7** was assessed by the colorimetric MTT assay with three human tumour cell lines, namely A2780 (ovarian carcinoma), MCF7 (breast adenocarcinoma) and MDAMB231 (breast adenocarcinoma derived from metastatic site). This panel of cell lines was selected in view of their different responses to cisplatin, the drug in clinical use, and taking also into account that they represent the most frequent cancer diseases diagnosed in women, *i.e.*, breast (MCF7, ERα+ and MDAMB231, ER-, PR-, HER2-) and ovarian (A2780) cancer conditions. The IC_{50} values were obtained from experiments performed after a 72 h treatment with the complexes within the 0.1 μM-200 μM concentration range. The IC_{50} values obtained for cisplatin were used for comparison. Results are summarized in **Table 3**. As can be observed, the presumably "spectator" coligand imparts impressive differences on the cytotoxic potency of the compounds. Compound **5**, bearing the DMSO coligand, was non-cytotoxic; replacing this ligand by CO, we obtained compound **6** that showed a moderate cytotoxicity against the ovarian cancer cells; finally, when the coligand is the triphenlyphosphane, the resulting compound **7**, was highly cytotoxic against all three cancer cell lines tested, as expected from our previous results with its analogue TM34, $[Ru(\eta^5\text{-}C_5H_5)(bipy)(PPh_3)][CF_3SO_3]$ [12,14]. Phosphane coligands, and particularly PPh_3, have been related to the increasing cytotoxicity on ruthenium based systems as recently reported for $[Ru(Cl)(PPh_3)(Lig\text{-}N)]$, $[Ru(Cl)_2(Lig\text{-}N)]$ (where Lig-N = pyridine derivate)

and [Ru(Cl)(PPh_3)$_2$] derivatives[26]. In this frame, the cytotoxic effect of the uncoordinated triphenylphosphane, was studied on MCF7 cancer cell line in the same experimental conditions as for complexes **5**-**7**. The results show that IC_{50} for uncoordinated PPh_3 is 112.6 ± 33 μM (**Figure S4**), showing that the strong cytotoxicity of compound **7** is, in fact a synergy between all the compound components, where the fragment {Ru(η^5-C_5H_5)} plays a crucial role on the electronic interactions. To sum up, the differences on the electronic activation of the bipy ligand (see above) imparted by the co-ligand structural diversity seem to have a direct correlation with the cytotoxic properties of the complexes.

Table 3.

2.6.2. In vitro studies with Human Serum Albumin (HSA)

Binding to HSA

HSA is the most important non-specific transport vehicle in the human blood plasma. Its important ability to bind both endogenous metabolic compounds and exogenous therapeutic drugs is well-known and strongly affects drug bioavailability and modifies the retention time *in vivo*[29-31]. The assessment of complex binding to HSA is an important first approach to drugs pharmacokinetics. In addition, due to the known enhanced permeability and retention effect (EPR effect) selective extravasation and retention of macromolecular drugs by solid tumours could be achieved[32]. In this context, HSA could potentially increase the cytotoxicity of complexes **5** and **6** through selective extravasation and retention by the tumour tissue[32]. Binding to HSA was investigated using fluorescence spectroscopy, using the intrinsic emission of HSA mainly due to its tyrosine and tryptophan residues. HSA contains a single tryptophan

moiety, Trp214 (located in the subdomain II.A), which can be selectively excited at λ_{exc} = 295 nm and used as an intrinsic structural probe in the protein[29,33]. Trp214 is very sensitive to its local environment and its emission easily reflects small changes in the vicinity of the indole ring [33], which makes it an attractive probe for detecting interactions between HSA and a metallodrug. In this study, fatty acid-free HSA was used to evaluate the binding ability of the protein for the ruthenium complexes **5**-**7**. The low solubility of these complexes required the use of a small amount of DMSO as a co-solvent. A DMSO content as low as 2% quenches the fluorescence emission of Trp214 in *ca.* 10% (no spectral shifts being observed). In this study, care was taken to add, at the same time, the same volume of DMSO to both "HSA alone" and "complex-HSA" samples, to ensure the same DMSO content in "HSA alone" solutions (prepared from stock solutions with no DMSO), in samples and in blanks. In HSA, the maximum emission intensity for albumin Trp214 is observed at 334 nm[33]. As an example, **Figure 7a** shows the effect of increasing concentrations of compound **5** on the protein emission: a quenching of the fluorescence intensity is observed, with no shift in the maximum λ_{em}. The same behaviour was observed for complexes **6** and **7**. All complexes exhibit a strong absorption band at 295 nm (λ_{exc}) that tails to the visible range, and absorbance is still considerably high at 340 nm (λ_{em} max, see **Figure 1**). Hence, data must be corrected for inner filter effects (IFE) at both excitation and emission wavelengths to account for a decrease in the fluorescence intensity that is not due to a real binding interaction[54,33]. The relative intensity emitted at 340 nm in the presence of complexes **5**-**7** and corrected for IFE is depicted in **Figure 7b**. This wavelength was chosen because it is near of the maximum emission wavelength (345 nm) but after the water Raman scattering peak, and the signal-to-background ratio is much more favourable than it would be if the actual maximum emission wavelength was used. It can be clearly seen in **Figure 7b** that the

presence of complexes **5**-**7** quenches the Trp214 emission in a concentration-dependent manner, which is consistent with binding to the protein (although real saturation conditions could not be attained due to solubility constrains). In addition, the extent of quenching observed is greater for complex **6** bearing the CO coligand.

The very small changes detected in the UV-Vis electronic spectrum of these compounds in the presence of the protein support the fact that the parent complex binds as a whole, with no loss of any of its coligands.

Figure 7.

Effect of HSA of the cytotoxicity of compounds 5 and 6

As explained above, serum proteins play a crucial role in the transport and delivery of antitumoral metallodrugs, and are frequently involved in their mechanism of action. In the prospective that the majority of metallodrugs are administered intravenously, interactions with HSA can be determinant for their biodistribution and can affect the drugs' biological activity. In this frame, the cytotoxic activity of the complexes **5** and **6** when bound to HSA was evaluated aiming at obtaining an increase in their anticancer activity. Experiments were carried out with MCF7 cells at 72 h incubation time. Several controls were used in these assays, namely cells with no treatment (negative control), cells treated with HSA alone and cells treated with complexes **5** and **6** in the absence of HSA. On the case of complex **5** (**Figure 8**), binding to HSA resulted in an increase of *ca.* 38% on the cytotoxic activity against MCF7 cells, probably as a result of a better uptake into the cells. However, one should not neglect that since this compound

presents a high IC_{50}, the quantities of HSA needed to achieve a 1:0.5 ratio are also high, causing by its turn a decrease on the cellular viability of the MCF7 cells. For complex **6**, the incubation with HSA had no effects on the cytotoxicity of the compound (**Figure 8**), indicating that the activity of the complex remains relatively unaffected when bound to HSA. These results show that the interaction of these complexes with HSA *in vivo* will likely have a positive outcome in what concerns activity.

Figure 8.

3. Conclusions

A new family of $[Ru(\eta^5\text{-}C_5H_5)(bipyridine)(L)][PF_6]$ complexes has been designed and synthesized in view to understand the role of the σ bonded coligands (L) in the cytotoxicity of the new compounds and to find possible structure-activity correlations. A set of compounds presenting N-bonded (**1**-**4**, imidazole derivatives), S-bonded (**5**, DMSO), C-bonded (**6**, CO) and P-bonded (**7**, PPh_3) coligands was studied and the spectroscopic, electrochemical and DFT data were correlated to understand the electronic features of these molecules. Taking all the results in consideration, it has been clearly shown that the coligand L has a crucial role in the fine-tuning of the electronic density at ruthenium centre as a result of their different π acceptor character. Thus, N-imidazole derivatives, DMSO and CO coligands pulled the electronic density from the $\{Ru(\eta^5\text{-}C_5H_5)(bipy)\}^+$ fragment via a π-backdonation interaction (the most drastic case was CO). The ability of coligand PPh_3 as π acceptor is not far from the other coligands, with the obvious exception of CO, when experimental data are compared, but surprisingly compound **7** showed higher electronic density on bipy rings. An explanation for this effect can possibly be accounted by the influence a phenyl ring current of the phosphane in the protons of bipyphenyl (see X ray

section) leading to a higher electronic density of at the bipy ligand. As consequence, the bipyridyl ligand might be more activated for expected electronic interactions with the charged cell membranes, which have been on the basis of the good anticancer performance of our {Ru(η^5-C_5H_5)} based family of compounds[28,34]. In good agreement with this evidence, from compounds **5**-**7**, compound **7** showed the best IC_{50} values for the ovarian (A2780) and breast (MCF7 and MDAMB231) human cancer cell lines. Instability in HEPES buffer excluded compounds **1**-**4** from this cytotoxic evaluation study. Although our studies do not lead to a straightforward conclusion about structure – activity relations one can foresee that for this general family of $[Ru(\eta^5\text{-}C_5H_5)(L)(bipy)]^+$ the best cytotoxic effect could be associated with a better electronic activation of the bipy as already observed in analogous compounds[55]. Thus, the coligand L can play an important role on this activation and it should certainly present remarkable σ donor and poor π acceptor abilities to boost the electronic activation at the bipyridyl ligand.

4. Experimental Section

4.1. General procedures

Fatty acid-free HSA (approx. 99%, lyophilized powder, A3782) was purchased from Sigma-Aldrich. Millipore® water was used for the preparation of all aqueous solutions, and 10 mM 4-(2-hydroxyethyl)-1-piperazineethanesulfonic acid (HEPES) buffer (Sigma-Aldrich) was used in all experiments involving spectroscopic measurements. This buffer system was adjusted to pH 7.4 using KOH and/or HCl solutions. All syntheses were carried out under dinitrogen atmosphere using current *Schlenk* techniques and the solvents used were dried using standard methods[35]. Starting material $[Ru(\eta^5\text{-}C_5H_5)(PPh_3)_2Cl]$ was prepared following the methods described in the literature[36]. FT-IR spectra were recorded in a Shimadzu IRAffinity-1

spectrophotometer controlled by Shymadzu's IRsolution software (version 1.60) with KBr pellets; only significant bands are cited in text. ^{1}H, ^{13}C and ^{31}P NMR spectra were recorded on a Bruker Avance 400 spectrometer at probe temperature. The ^{1}H and ^{13}C chemical shifts are reported in parts per million (ppm) downfield from internal Me_4Si and the ^{31}P NMR spectra are reported in ppm downfield from external standard, 85% H_3PO_4. Elemental analyses were obtained at *Laboratório de Análises* from *Instituto Superior Técnico*. Electronic spectra were recorded at room temperature on a Jasco V-660 spectrophotometer controlled by Jasco's spectra manager (version 2.09) in the range of 190-900 nm.

4.2. Complexes syntheses

$[Ru(\eta^5\text{-}C_5H_5)(NCCH_3)_3][PF_6]$ synthesis was adapted from [37]. Briefly, benzeneruthenium(II) chloride dimer (1.0 g, 2.0 mmol) was added to a 500 mL round bottomed flask and dissolved in ≈ 300 mL of acetonitrile. To the brick red solution was added freshly synthesized sodium cyclopentadiene (464 mg, 4.0 mmol). After stirring over night at r.t., the reaction was filtered through Celite and the solvent evaporated. The resulting compound was then taken up in the minimum volume of water. To this solution a saturated aqueous solution of KPF_6 was added and the product was vigorously extracted into dichloromethane. The organic phase was evaporated to give a light brownish solid which was dissolved in ≈ 800 mL of acetonitrile and irradiated with a UV-light for 4 h. Finally, the solvent was removed under vacuum to give a brown product (yield ≈ 50%).

General procedure applied to the synthesis of complexes 1-4

$[Ru(NCCH_3)_3][PF_6]$ (0.3 mmol) were dissolved in dichloromethane (≈ 20 mL). The solution was cooled down to 0 ºC and then 0.3 mmol of 2,2-bipyridine were added. After stirring the solution for ≈ 5 min at this temperature, the ice-bath was removed and the solution was stirred for an

additional 30 min, followed by the addition of 0.3 mmol of the adequate ligand (L_1 = ImH; L_2 = 1-BI; L_3 = 4-IMP; L_4 = 1-MPI). The resulting solution was filtered through Celite and reduced in volume. *n*-Hexane was added to precipitate the compounds as orange/red products.

[Ru(η^5-C_5H_5)(2,2-bipy)(imidazole)][PF_6], 1

Orange; Yield = 71 %. Recrystallized from CH_2Cl_2/*n*-hexane. IR (KBr, cm^{-1}): ν(C-H aromatics) 3140-3000, ν(C-C aromatics) 1600-1400, ν(C-N) 1400-1200, ν(PF_6^-) 842 and 557. ^{1}H NMR ($(CD_3)_2CO$, Me_4Si, δ/ppm): 11.68 (s, 1, NH); 9.88 (d, 2, H_d; $^3J_{HH}$ = 5.6 Hz); 8.47 (d, 2, H_a; $^3J_{HH}$ = 8.4 Hz); 8.07 (t, 2, H_b; $^3J_{HH}$ = 7.8 Hz); 7.72 (s, 1, H_2); 7.63 (t, 2, H_c; $^3J_{HH}$ = 6.6 Hz); 7.07 (s, 1, H_5); 6.60 (s, 1,H_4); 4.48 (s, 5, η^5-C_5H_5); ^{13}C NMR ($(CD_3)_2CO$, Me_4Si, δ/ppm): 156.7 (C_e); 156.6 (C_d); 139.0 (C_2); 137.3 (C_b); 130.4 (C_4); 127.0 (C_c); 123.9 (C_a); 118.5 (C_5); 71.9 (η^5-C_5H_5); ^{31}P($(CD_3)_2CO$, δ/ppm): -144.27 (setp, PF_6^-). UV-Vis in CH_2Cl_2, λmax/nm (ε/$M^{-1}cm^{-1}$): 244 (15280), 296 (24472), 345 (4788), 465 (3991), 511 (*Sh*). UV-Vis in NCMe, λmax/nm (ε/$M^{-1}cm^{-1}$): 209 (*Sh*), 242 (14577), 295 (23124), 341 (4428), 462 (3704). UV-Vis in DMSO, λmax/nm (ε/$M^{-1}cm^{-1}$): 298 (23300), 345 (4591); 469 (3754). Elemental analysis (%) Found: C 39.4, H 3.2, N 9.8. Calc. for $C_{18}H_{17}F_6N_4PRu$•⅓CH_2Cl_2: C 39.1, H 3.2, N 9.9.

[Ru(η^5-C_5H_5)(2,2-bipy)(1-Benzylimidazole)][PF_6], 2

Dark red; Yield: 80 %. Recrystallized from CH_2Cl_2/*n*-hexane. IR (KBr, cm^{-1}): ν(C-H aromatics) 3130-3000, ν(C-C aromatics) 1600-1400, ν(C-N) 1400-1200, ν(PF_6^-) 839 and 555. ^{1}H NMR ($(CD_3)_2CO$, Me_4Si, δ/ppm): 9.83 (d, 2, H_d; $^3J_{HH}$ = 4 Hz); 8.46 (d, 2, H_a; $^3J_{HH}$ = 7.6 Hz); 8.07 (t, 2, H_b; $^3J_{HH}$ = 7 Hz); 7.83 (s, 1, H_2); 7.61 (t, 2, H_c; $^3J_{HH}$ = 7 Hz); 7.29 (m, 3, H_5+H_8+H_{12}); 7.03 (m, 3, H_9+H_{10}+H_{11}); 6.51 (s, 1, H_4); 5.12 (s, 2, H_6); 4.47 (s, 5, η^5- C_5H_5); ^{13}C NMR ($(CD_3)_2CO$, Me_4Si, δ/ppm): 157.11 (C_e); 156.65 (C_d); 140.79 (C_2); 137.44 (C_7); 137.35 (C_c); 131.29 (C_4);

129.83 (C_8, C_{12}); 129.16 (C_{10}); 128.35 (C_9, C_{11}); 127.14 (C_b); 123.89 (C_a); 121.86 (C_5); 72.01 (η^5- C_5H_5); 51.76 (C_6). ^{31}P RMN ($(CD_3)_2CO$, δ/ppm): -144.24 (setp, PF_6^-). UV-Vis in CH_2Cl_2, λmax/nm (ε/$M^{-1}cm^{-1}$): 244 (15978); 296 (23176); 345 (4781); 465 (3702). UV-Vis in NCMe, λmax/nm (ε/$M^{-1}cm^{-1}$): 242 (15575); 294 (23377); 341 (4555); 461 (3711); UV-Vis in DMSO, λmax/nm (ε/$M^{-1}cm^{-1}$): 298 (23596); 345 (4559); 466 (3802). Elemental analysis (%) Found: C 47.1, H 3.6, N 8.7. Calc. for $C_{25}H_{23}F_6N_4PRu \cdot {}^1/_5 CH_2Cl_2$: C 47.1, H 3.7, N 8.7.

Ru(η^5-C_5H_5)(2,2-bipy)(4-(1-imidazolyl)-phenol)][PF_6], 3

Dark red; Yield: 79%. Recrystallized from NCMe/diethyl ether and CH_2Cl_2/*n*-hexane. IR (KBr, cm^{-1}): ν(C-H aromatics) 3140-3000, ν(C-C aromatics) 1600-1400, ν(C-N) 1400-1200, ν(C-O) 1247, ν(PF_6^-) 842 and 555. ^{1}H NMR ($(CD_3)_2CO$, Me_4Si, δ/ppm): 9.90 (d, 2, H_d; $^3J_{HH}$ = 5.6 Hz); 8.76 (s, 1, OH); 8.48 (d, 2, H_a; $^3J_{HH}$ = 8.0 Hz); 8.19 (s, 1, H_2); 8.08 (t, 2, H_b; $^3J_{HH}$ = 7.8 Hz); 7.63 (t, 2, H_c; $^3J_{HH}$ = 6.6 Hz); 7.36 (s, 1, H_5); 7.25 (d, 2, H_8+H_{10}; $^3J_{HH}$ = 8.4 Hz); 6.90 (d, 2, H_7+H_{11}; $^3J_{HH}$ = 8.8 Hz); 6.55 (d, 1, H_4); 4.51 (s, 5, η^5- C_5H_5). ^{13}C NMR ($(CD_3)_2CO$, Me_4Si, δ/ppm): 158.37 (C_9); 157.10 (C_e); 156.70 (C_d); 139.09 (C_2); 137.36 (C_b); 131.25 (C_4); 129.47 (C_6); 127.17 (C_c); 123.88 (C_8+C_{10}); 120.82 (C_5); 117.16 (C_7+C_{11}); 72.00 (η^5- C_5H_5). ^{31}P NMR ($(CD_3)_2CO$, δ/ppm): -144.21 (setp, PF_6^-). UV-Vis in CH_2Cl_2, λmax/nm (ε/$M^{-1}cm^{-1}$): 242 (24500), 295 (29700), 345 (5380), 464 (4390), 508 (*Sh*). UV-Vis in NCMe, λmax/nm (ε/$M^{-1}cm^{-1}$): 241 (23300), 293 (28900), 339 (4750), 460 (3840). UV-Vis in DMSO, λmax/nm (ε/$M^{-1}cm^{-1}$): 297 (27800), 341 (4920), 466 (3820). Elemental analysis (%) Found: C 45.5, H 3.3, N 8.8. Calc. for $C_{24}H_{21}F_6N_4OPRu$: C 45.9, H 3.4, N 8.9.

[Ru(η^5-C_5H_5)(2,2-bipy)(1-(4-methoxyphenyl)-1H-imidazole)][PF_6], 4

Dark red; Yield: 82%. Recrystallized from NCMe/diethyl ether. IR (KBr, cm^{-1}): ν(OH) 3530, ν(C-H aromatics) 3140-3000, ν(C-C aromatics) 1600-1400, ν(C-N) 1400-1200, ν(PF_6^-) 840 and 560. ^{1}H RMN ($(CD_3)_2CO$, Me_4Si, δ/ppm): 9.90 (d, 2, H_d; $^3J_{HH}$ = 5.6 Hz); 8.49 (d, 2, H_a; $^3J_{HH}$ = 8.0 Hz); 8.27 (s, 1, H_2); 8.08 (t, 2, H_b; $^3J_{HH}$ = 7.8 Hz); 7.64 (t, 2, H_c; $^3J_{HH}$ = 6.4 Hz); 7.42 (s, 1, H_5); 7.40 (d, 2, H_8+H_{10}; $^3J_{HH}$ = 8.8 Hz); 7.02 (d, 2, H_7+H_{11}; $^3J_{HH}$ = 8.8 Hz); 6.55 (s, 1, H_4); 4.52 (s, 5, η^5- C_5H_5); 3,81 (s, 3, H_{12}). ^{13}C NMR ($(CD_3)_2CO$, Me_4Si, δ/ppm): 160.46 (C_9); 157.07 (C_e); 156.69 (C_d); 139.15 (C_2); 137.35 (C_b); 131.28 (C_4); 130.05 (C_6); 127.16 (C_c); 123.87 (C_8+C_{10}); 123.66 (C_a); 120.75 (C_5); 115.79 (C_7+C_{11}); 72.00 (η^5- C_5H_5); 56.07 (C_{12}). ^{31}P RMN ($(CD_3)_2CO$, δ/ppm): -144.26 (setp, PF_6^-). UV-Vis in CH_2Cl_2, λmax/nm (ε/$M^{-1}cm^{-1}$): 241 (24900), 295 (27400), 345 (4630), 464 (3680), 513 (*Sh*). UV-Vis in NCMe, λmax/nm (ε/$M^{-1}cm^{-1}$): 241 (26700), 293 (29200), 339 (4990), 460 (3940). UV-Vis in DMSO, λmax/nm (ε/$M^{-1}cm^{-1}$): 297 (30000), 340 (4800), 465 (3540). Elemental analysis (%) Found: C 44.9, H 3.6, N 8.1. Calc. for $C_{25}H_{23}F_6N_4OPRu$•½CH_2Cl_2: C 44.8, H 3.5, N 8.2.

Synthesis of [Ru(η^5-C_5H_5)(2,2-bipy)(dmso)][PF_6], 5

0.3 mmol of [Ru(η^5-C_5H_5)($NCCH_3$)$_3$][PF_6] were dissolved in dichloromethane (≈ 20 mL). The solution was cooled down to 0 ºC and then 0.3 mmol of 2,2-bipyridine were added. After stirring the solution for ≈ 5 min at this temperature, the ice-bath was removed and the solution was stirred for an additional 30 min. Then, the dichloromethane was evaporated and the remaining product was dissolved in 200 µL of DMSO. After, *ca.* of 15 mL of deionized water were added and the solution was stirred for 30 min. The solution was filtered and the water was co-evaporated with diethyl ether. A recrystallization from CH_2Cl_2/diethyl ether was performed using the remaining solution, allowing the precipitation of the product.

Yellow; Yield: 70%. IR (KBr, cm^{-1}): ν(C-H η^5-C_5H_5) 3130, ν(CH_3) 2920, ν(S=O) 1094, ν(PF_6^-) 840 and 557. ^{1}H NMR ($(CD_3)_2CO$, Me_4Si, δ/ppm): 9.57 (d, 2, H_d; $^3J_{HH}$ = 5.6 Hz); 8.60 (d, 2, H_a; $^3J_{HH}$ = 8.4 Hz); 8.20 (t, 2, H_b; $^3J_{HH}$ = 8.0 Hz); 7.64 (t, 2, H_c; $^3J_{HH}$ = 6.6 Hz); 4.99 (s, 5, η^5-C_5H_5); 3.12 (s, 6, -CH_3). ^{13}C NMR ($(CD_3)_2CO$, Me_4Si, δ/ppm): 157.59 (C_e); 157.57 (C_d); 138.72 (C_b); 127.02 (C_a); 124.30 (C_c); 78.11 (η^5-C_5H_5); 49.78 (-CH_3). ^{31}P NMR ($(CD_3)_2CO$, δ/ppm): -144.27 (setp, PF_6^-). UV-Vis in CH_2Cl_2, λmax/nm (ε/$M^{-1}cm^{-1}$): decomposition along time. UV-Vis in NCMe, λmax/nm (ε/$M^{-1}cm^{-1}$): 238 (6820), 288 (11099); 385 (1743), 445 (*Sh*). UV-Vis in DMSO, λmax/nm (ε/$M^{-1}cm^{-1}$): 292 (16314); 389 (2776), 445 (*Sh*). Elemental analysis (%) Found: C 37.2, H 3.5, N 5.1. Calc. for $C_{17}H_{19}F_6N_2OPRuS$: C 37.4, H 3.5, N 5.1.

Synthesis of [Ru(η^5-C_5H_5)(2,2-bipy)(CO)][PF_6], <u>6</u>

0.3 mmol of [Ru(η^5-C_5H_5)($NCCH_3$)$_3$][PF_6] were dissolved in dichloromethane (≈ 20 mL). The solution was cooled down to 0 ºC and then 0.3 mmol of 2,2-bipyridine were added. After stirring the solution for ≈ 5 min at this temperature, the ice-bath was removed and the solution was stirred for an additional 30 min, followed by the addition of CO as a slow stream of this gas passing through the solution for ≈ 20 min at r.t.. The resulting solution was filtered through Celite and reduced in volume. *n*-Hexane was added to precipitate the compound as an orange product.

Orange; Yield: 60%. Recrystallized from MeOH/diethyl ether. IR (KBr, cm^{-1}): ν(C-H η^5-C_5H_5) 3125, ν(C=O) 1970, ν(PF_6^-) 840 and 557. ^{1}H NMR (MeOD, Me_4Si, δ/ppm): 9.10 (d, 2, H_d; $^3J_{HH}$ = 5.6 Hz); 8.54 (d, 2, H_a; $^3J_{HH}$ = 8.0 Hz); 8.22 (t, 2, H_b; $^3J_{HH}$ = 8.0 Hz); 7.56 (t, 2, H_c; $^3J_{HH}$ = 6.6 Hz); 5.34 (s, 5, η^5-C_5H_5). ^{13}C NMR (MeOD, Me_4Si, δ/ppm): 158.82 (C_d); 157.91 (C_e); 140.46 (C_b); 127.59 (C_c); 125.18 (C_a); 84.52 (η^5-C_5H_5). ^{1}H NMR (CD_3CN, Me_4Si, δ/ppm): 9.00 (d, 2, H_d); 8.38 (d, 2, H_a); 8.15 (t, 2, H_b); 7.51 (t, 2, H_c); 5.26 (s, 5, η^5-C_5H_5). ^{31}P NMR (MeOD,

δ/ppm): -144.57 (setp, PF_6^-). UV-Vis in CH_2Cl_2, λmax/nm (ε/$M^{-1}cm^{-1}$): 245 (10200); 287 (9000); 312 (6110); 341 (*Sh*); 460 (*Sh*). UV-Vis in NCMe, λmax/nm (ε/$M^{-1}cm^{-1}$): 245 (9610); 288 (8500); 311 (5820); 349 (Sh); 460 (*Sh*). UV-Vis in DMSO, λmax/nm (ε/$M^{-1}cm^{-1}$): 293 (8010); 315 (6040); 354 460 (*Sh*). Elemental analysis (%) Found: C 39.7, H 2.9, N 5.0. Calc. for $C_{16}H_{13}F_6N_2OPRu$: $C_{16}H_{13}F_6N_2OPRu•1/5C_4H_{10}O$: C 39.6, H 3.0, N 5.5.

Synthesis of complex [Ru(η^5-C_5H_5)(2,2-bipy)(PPh_3)][PF_6], 7

To a solution of [Ru(η^5-C_5H_5)(PPh_3)$_2$Cl] (150 mg, 0.21 mmol) in ≈ 30 mL of CH_2Cl_2 bipyridine (45 mg; 0.21 mmol) was added, followed by $AgPF_6$ (53 mg, 0.21 mmol). The reaction proceeded under reflux for 3 h leading to a dark orange solution and a white precipitate of AgCl. The solution was separated from the precipitate of AgCl by cannula-filtration and the solvent was removed by vacuum. The residue was recrystallized from dichloromethane/*n*-hexane.

Orange; Yield: 90%. IR (KBr, cm^{-1}): ν(C-H aromatics) 3140-3000, ν(C-C aromatics) 1600-1400, ν(C-N) 1400-1200, ν(PF_6^-) 839 and 556. ^{1}H NMR ($(CD_3)_2CO$, Me_4Si, δ/ppm): 9.50 (d, 2, H_d; $^3J_{HH}$ = 5.6 Hz); 8.17 (d, 2, H_a; $^3J_{HH}$ = 8.0 Hz); 7.90 (t, 2, H_b; $^3J_{HH}$ = 7.8 Hz); 7.42 (m, 3, $H_{para}(PPh_3)$); 7.32 (m, 8, H_c+$H_{meta}(PPh_3)$), 7.12 (m, 6, $H_{orto}(PPh_3)$); 4.92 (s, 5, η^5-C_5H_5). ^{13}C NMR ($(CD_3)_2CO$, Me_4Si, δ/ppm): 157.11 (C_d); 156.65 (C_e); 137.07 (C_b); 133.85, 133.74 (CH, PPh_3); 132.63, 132.22 (C_q, PPh_3); 129.41, 129.32 (CH, PPh_3); 125.93 (C_c); 124.22 (C_a); 79.39 (η^5-C_5H_5). ^{31}P NMR ($(CD_3)_2CO$, δ/ppm): 51.32 (s, PPh_3); -144.25 (setp, PF_6^-). UV-Vis in CH_2Cl_2, λmax/nm (ε/$M^{-1}cm^{-1}$): 238 (*Sh*) 291 (20785); 341 (*Sh*); 422 (3782); 470 (*Sh*); UV-Vis in NCMe, λmax/nm (ε/$M^{-1}cm^{-1}$): 228 (*Sh*); 290 (17440); 342 (*Sh*); 414 (3209); 468 (*Sh*); UV-Vis in DMSO, λmax/nm (ε/$M^{-1}cm^{-1}$): 293 (20330); 342 (*Sh*); 418 (3619); 470 (*Sh*). Elemental analysis (%) Found: C 51.0, H 3.8, N 3.4. Calc. for $C_{33}H_{28}F_6N_2P_2Ru•0.8CH_2Cl_2$: C 50.9, H 3.7, N 3.5.

Synthesis of complex [Ru(η^5-C_5H_5)(2,2-bipy)($NCCH_3$)][PF_6], 8

This compound, used as intermediate in the synthesis of compounds **1**-**7** was isolated and charaterized in view to confirm some observations found in the electrochemical experiments. 0.3 mmol of [Ru(η^5-C_5H_5)($NCCH_3$)$_3$][PF_6] were dissolved in dichloromethane (≈ 20 mL). The solution was cooled down to 0 ºC and then 0.3 mmol of 2,2-bipyridine were added. After stirring the solution for ≈ 5 min at this temperature, the ice-bath was removed and the solution was stirred for an additional 30 min**.** After solvent evaporation under vacuum the compound was recrystallized from acetonitrile/diethyl ether to give an orange product. Yield: 40%. ^{1}H NMR (CD_3CN, Me_4Si, δ/ppm): 9.47 (d, 2, H_d); 8.28 (d, 2, H_a); 8.01 (t, 2, H_b); 7.49 (t, 2, H_c), 4.42 (s, 5, η^5-C_5H_5), 1.96 (s, 3, CH_3). ^{31}P NMR (CD_3CN, δ/ppm): -144.64 (setp, PF_6^-).

4.3. X-ray crystal structure determination

Three-dimensional X-ray data for [Ru(η^5-C_5H_5)(bipy)PPh_3][PF_6]·$(CH_3)_2CO$ 7 were collected on a Bruker SMART Apex CCD diffractometer at 100(2) K, using a graphite monochromator and Mo-K_α radiation (λ = 0.71073 Å) by the ϕ-ω scan method. Reflections were measured from a hemisphere of data collected of frames each covering 0.5 degrees in ω. Of the 265907 reflections measured in 7, all of which were corrected for Lorentz and polarization effects, and for absorption by semi-empirical methods based on symmetry-equivalent and repeated reflections, 8335 independent reflections exceeded the significance level $|F|/\sigma(|F|) > 4.0$, respectively. Complex scattering factors were taken from the program package SHELXTL[38]. The structure was solved by direct methods and refined by full-matrix least-squares methods on F^2. The non-hydrogen atoms were refined with anisotropic thermal parameters in all cases. Hydrogen atoms were located in difference Fourier map and left to refine freely, except for C(2S), C(3SA),

C(3SB), C(3) and C(4), which were included in calculation positions and refined in the riding mode. A final difference Fourier map showed no residual density outside: 0.986 and -0.783 e.Å^{-3}. A weighting scheme w = $1/[\sigma^2(F_o^2) + (0.049500\ P)^2 + 7.468500\ P]$ for **7**, where P = $(|F_o|^2 + 2|F_c|^2)/3$, were used in the latter stages of refinement. The crystal presents a slight disorder on the acetone molecule. This disorder has been refined and two atomic sites for one carbon atom and oxygen atom of the acetone molecule have been observed and refined with the anisotropic atomic displacement parameters. The site occupancy factor was 0.45910 for C(3SA) and O(1SA). CCDC No. &&& contain the supplementary crystallographic data for **7**. These data can be obtained free of charge via http://www.ccdc.cam.ac.uk/conts/retrieving.html, or from the Cambridge Crystallographic Data Centre, 12 Union Road, Cambridge CB2 1EZ, UK; fax: (+44) 1223-336-033; or e-mail: deposit@ccdc.cam.ac.uk. Crystal data and details of the data collection and refinement for the new compounds are collected in **Table 4**.

Table 4.

4.4. Electrochemical experiments

The electrochemical experiments were performed on an EG&G Princeton Applied Research Model 273A potentiostat/galvanostat and monitored with the Electrochemistry PowerSuite v2.51 software from Princeton Applied Research. Cyclic voltammograms were obtained in 0.1 M or 0.2 M solutions of $[NBu_4][PF_6]$ in NCMe or CH_2Cl_2 respectively, using a three-electrode configuration cell with a platinum-disk working electrode (1.0 mm diameter) probed by a Luggin capillary connected to a silver-wire pseudo-reference electrode and a Pt wire counter electrode. The electrochemical experiments were performed under a dinitrogen atmosphere at room temperature. The redox potentials were measured in the presence of ferrocene as the internal

standard and the redox potential values are normally quoted relative to the SCE by using the ferrocenium/ferrocene redox couple ($E_{1/2}$ = 0.46 or 0.40 V *vs.* SCE for CH_2Cl_2 or NCMe, respectively). The supporting electrolyte was purchased from Fluka (electrochemical grade), dried under vacuum for several hours and used without further purification. Reagent grade acetonitrile and dichloromethane were dried over P_2O_5 and CaH_2, respectively and distilled under dinitrogen atmosphere before use.

4.5. DFT Calculations

All calculations were performed at the DFT level of theory using Thrular's M06-L functional as implemented in Gaussian09[39-41]. The choice of this functional was due to its outstanding performance and low computational cost[42]. The LANL2DZ effective core potential basis set was used for heavy atoms (S, P and Ru) [43,44]. Geometry optimizations were made in the gas-phase without any symmetry constrains. The nature of the stationary points was evaluated by computing the Hessian matrix. No imaginary frequencies were obtained.

TD-DFT was used in combination with the PCM solvation model in order to compute the electronic spectra of the studied molecules[45-47]. TD-DFT calculations were made applying the same theory level and basis sets used for the calculation of the geometries. The first 120 lower excitation energies were computed, and the simulated absorption bands were obtained by convolution of Gaussian functions centred at the calculated excitation energies using the QMforge software[48]. The Chemcraft 80 program was used for the visualization of the remaining computed results[49].

4.6. Stability studies in HEPES buffer

For the stability studies, all the complexes were dissolved in 2-3% DMSO / 98-97% HEPES buffer (pH = 7.4) at *ca.* 1×10^{-4} M and their electronic spectra were recorded in the range allowed by the solvents at set time intervals.

4.7. Sample preparation of complex—HSA complexes

Stock solutions of human serum albumin were prepared by gently dissolving the protein in 10 mM HEPES buffer (4-(2-Hydroxyethyl)piperazine-1-ethanesulfonic acid, pH 7.4). The protein concentration was determined by UV spectrophotometry using the molar absorption coefficient ε (280 nm) = 36850 M^{-1} cm^{-1}[50,51]. First a concentrated stock solution of the complex was prepared in HEPES with 2% of DMSO (from Sigma-Aldrich). Then, individual protein-complex samples were prepared by mixing a fixed volume of protein solution with different volumes of the complex stock solution, followed by a dilution with HEPES (containing 2% of DMSO) for a final volume of 4 mL. For fluorescence measurements, the final protein concentration was 2.0 μM, and the complex concentrations ranged from 0 – 45 μM. Sample solutions were homogenized and left in an incubator at (37 ± 1) ºC for 24 ± 3h to ensure equilibrium conditions were attained before measurement.

4.8. Fluorescence spectroscopic measurements

Steady state fluorescence measurements were carried out on a Spex Fluorolog® 3-22/Tau-3 spectrofluorometer from Horiba Jobin Yvon at (37 ± 1 ºC) equipped with a 1.0 cm quartz cell. The excitation and emission slit widths were fixed at 4.0 nm. The excitation wavelength was 295 nm to selectively excite the lone Trp214 residue, and its emission spectra were recorded from 310 to 550 nm. For these measurements, the final protein concentration in the samples was 2.0 μM (constant), and the complex concentration was varied accordingly to obtain HSA-to-Ru-complex molar ratios ranging from 1:0.5 to 1:25. Incubation time was (24 ± 3) h at 37 °C.

Samples with the same complex concentration but no protein were also prepared for appropriate background correction. The fluorescence intensities were corrected for the inner filter effect due to the absorption of the exciting light and reabsorption of the emitted light[52-54] with UV-Vis absorption data recorded for each sample on a Jasco V-560 spectrophotometer in the range of 250 to 600 nm with 1 cm path quartz cells.

4.9. Cell viability assays in human tumour cell lines

A2780 ovarian, MCF7 and MDAMB231 breast cancer human tumor cell lines (ATCC) were grown in cell culture flasks in a 5% CO_2 incubator at 37 °C with humidified atmosphere (Heraeus, Germany). The culture media RPMI (A2780) and DMEM with Glutamax I (MCF7 and MDAMB231) was supplemented with 10% FBS (fetal bovine serum) and 1% penicillin/streptomycin. The cells were adherent in monolayers and, upon confluence, were harvested by digestion with trypsin-EDTA (Gibco). The cytotoxicity of the Ru complexes against the tumour cells was assessed using the colorimetric assay based on the reduction of the tetrazolium dye MTT by viable cells. For this purpose, cells ($10–20\times10^3$ / 200 μL medium) were seeded into 96-well plates and incubated for 24 h (37 °C/5% CO_2) for cell adherence. Compounds were dissolved in DMSO and then in medium and added to the cells in serial dilutions ranging from 0.1 μM to 200 μM. The final concentration of DMSO in medium did not exceed 1%. After 72 h incubation, the treatment solution was discarded and a MTT solution (200 μL, 0.5 mg/mL PBS – phosphate buffered saline) was added to each well. After 3–4 h at 37 °C/5% CO_2, the solution was removed and the purple formazan crystals formed inside the cells were dissolved in 200 μL DMSO by thorough shaking. The absorbance of the resulting solutions was measured at 570 nm using an ELISA reader (PowerWave Xs, Bio-Tek Instruments, Winooski, VT, USA). The measured absorbance was then converted to percentage cellular

viability relative to the control samples (cells without treatment). The cytotoxic effects of the compounds were quantified calculating the IC_{50} values, based on non-linear regression analysis of the dose response (percentage cellular viability) data (GraphPad Prism software).

4.10. Effect of HSA on the cytotoxicity of compound 5-6

The effect of albumin (HSA) on cell viability of MCF7 cells, either alone or in combination with 5 and 6, was evaluated using a complex concentration equivalent to the IC_{50} values obtained at 72 h incubation and at compound-to-protein molar ratio of 1:0.5. The complexes were pre-incubated with HSA in medium containing only 5% of FBS for 20 min at 37 °C and then added to the cells.[56]. After a 72 h incubation period the treatment solution was removed, and the cell viability was measured by the MTT assay.

Acknowledgements

This work was financed by national funds through FCT, the Portuguese Foundation for Science and Technology, within the scope of projects PTDC/QUI-QUI/118077/2010 and PEst-UID /QUI/00100/2013. Andreia Valente and Ana Isabel Tomaz thank the Investigator FCT2013 initiative for projects IF/01302/2013 and IF/01179/2013, respectively.

References

[1] C.S. Allardyce, P.J. Dyson, Platinum Metals Rev.45 (2001) 62-69.

[2] P.C.A. Bruijnincx, P.J. Sadler, J. Curr. Opin. Chem. Biol.12 (2008) 197-206.

[3] E. Alessio, G. Mestroni, A. Bergamo, G. Sava, Curr. Topics Med. Chem. 4 (2004) 1525-1535.

[4] C.G. Hartinger, M.A. Jakupec, S. Zorbas-Seifrieda, M. Groessl, A. Egger, W. Berger, H. Zorbas, P.J. Dyson, B.K. Keppler, Chem. Biodivers. 5 (2008) 2140–2155.

[5] G. Sava, E. Alessio, A. Bergamo, G. Mestroni, in: Clarke, M.J.; Sadler, P.J. (Eds.), Metallopharmaceuticals I: DNA Interactions, Springer, 1999, pp. 143-169.

[6] C. Scolaro, A. Bergamo, L. Brescacin, R. Delfino, M. Cocchietto, G. Laurenczy, T.J. Geldbach, G. Sava, P.J. Dyson, J. Med. Chem. 48 (2005) 4161–4171.

[7] P.C.A. Bruijnincx, P.J. Sadler in: van Eldik, R.; Hubbard, C.D. (Eds.), Advances in Inorganic Chemistry, 61, Academic Press, London, 2009, pp. 1–62.

[8] R. Anand, J. Maksimoska, N. Pagano, E.Y. Wong, P.A. Gimotty, S.L. Diamond, E. Meggers, R. Marmorstein, J. Med. Chem. 52 (2009) 1602–1611.

[9] E. Meggers, G.E. Atilla-Gokcumen, K. Gründler, C. Frias, A. Prokop, A. Dalton Trans. (2009) 10882–10888.

[10] M.H. Garcia, T.S. Morais, P. Florindo, M.F.M. Piedade, V. Moreno, C. Ciudad, V. Noe, J. Inorg. Biochem. 103 (2009) 354-361.

[11] V. Moreno, J. Lorenzo, F.X. Aviles, M.H. Garcia, J.P. Ribeiro, T.S. Morais, P. Florindo, M.P. Robalo, Bioinorg. Chem. Appl. 2010, Article ID 936834, 11 pages.

[12] V. Moreno, M. Font-Bardia, T. Calvet, J. Lorenzo, F.X. Avilés, M.H. Garcia, T.S. Morais, A. Valente, M.P. Robalo, J. Inorg. Biochem. 105 (2011) 241–249.

[13] T.S. Morais, T.J.L. Silva, F. Marques, M.P. Robalo, F. Avecilla, P.J.A. Madeira, P.J.G. Mendes, I. Santos, M.H. Garcia, J. Inorg. Biochem. 114 (2012) 65-74.

[14] A.I. Tomaz, T. Jakusch, T.S. Morais, F. Marques, R.F.M. Almeida, F. Mendes, E.A. Enyedy, I. Santos, J.C. Pessoa, T. Kiss, M.H. Garcia, J Inorg Biochem. 117 (2012) 261-269.

[15] T.S. Morais, F. Santos, L. Côrte-Real, F. Marques, M.P. Robalo, P.J.A. Madeira, M.H. Garcia, J. Inorg. Biochem. 122 (2013) 8-17.

[16] A. Valente, M.H. Garcia, F. Marques, Y. Miao, C. Rousseau, P. Zinck, J. Inorg. Biochem. 127 (2013) 79-81.

[17] I. Ferrer, J. Rich, X. Fontrodona, M. Rodríguez, I. Romero, Dalton Trans. 42 (2013) 13461-13469.

[18] I. Bratsos, C. Simonin, E. Zangranado, T. Gianferrara, A. Bergamo, E. Alessio, Dalton Trans. 40 (2011) 9533.

[19] M.K. Smith, J.A. Gibson, C.G. Young, J.A. Broomhead, P.C. Junk, F.R. Keene, Eur. J. Inorg. Chem. (2000) 1365-1370.

[20] J. Mola, M. Romero, M. Rodríguez, F. Bozoglian, A. Poater, M. Solà, T. Parella, J. Benet-Buchholz, X. Fontrodona, A. Llobet, Inorg. Chem. 46 (2007) 10707-10716.

[21] F.D. Rochon, C. Bensimon, C. Tessier, Inorg. Chim. Acta 361 (2008) 16-28.

[22] K. Nakamoto, in Infrered and Raman Spectra of Inorganic and Coordination Compounds, Part B, 6th Edition, WILEY-VCH, Hoboken, New Jersey, 2009, pp. 107-109.

[23] N. Mina-Camilde, I.C. Manzanares, J.F. Caballero, J. Chem. Ed. 173 (1996) 804-807.

[24] P.J.A. Madeira, T.S. Morais, T.J.L. Silva, P. Florindo, M.H. Garcia, Rapid Communications in Mass Spectrometry 26 (2012) 1675-1686.

[25] P. Govindaswamy, D. Linder, J. Lacour, G. Süss-Fink, B. Therrien, Dalton Trans. (2007) 4457-4463.

[26] R. Sáez, J. Lorenzo, M.J. Prieto, M. Font-Bardia, T. Calvet, N. Omeñaca, M. Vilaseca, V. Moreno, J. Inorg. Biochem. 136 (2014) 1-12.

[27] S. Gama, F. Mendes, T. Esteves, F. Marques, A. Matos, J. Rino, J. Coimbra, M. Ravera, E. Gabano, I. Santos, A. Paulo, Chem. Bio. Chem. 13 (2012) 2352-2362.

[28] L. Côrte-Real, A.P. Matos, I. Alho, T.S. Morais, A.I. Tomaz, M.H. Garcia, I. Santos, M.P. Bicho, F. Marques, Microsc Microanal. 19 (2013) 1122-1130.

[29] J. C. Pessoa, I. Tomaz, Curr. Med. Chem. 17 (2010) 3701–3738.

[30] G. Colmenarejo, Med. Res. Rev. 23 (2003) 275–301.

[31] M. Fasano, S. Curry, E. Terreno, M. Galliano, G. Fanali, P. Narciso, S. Notari, P. Ascenzi, IUBMB Life 57 (2005) 787–796.

[32] F. Kratz, J. Control. Rel. 132 (2008) 171–183.

[33] J.R. Lakowicz, "Principles of Fluorescence Spectroscopy" Third Edition, 2006, Springer.

[34] L. Côrte-Real, F. Mendes, J. Coimbra, T.S. Morais, A.I. Tomaz, A. Valente, M.H. Garcia, I. Santos, M. Bicho, F. Marques, J. Biol. Inorg. Chem. 2014.

[35] D.D. Perrin, W.L.F. Amarego, D.R. Perrin, Purification of Laboratory Chemicals, 2nd Ed., Pergamon, New York, 1980, pp. 65-371.

[36] M.I. Bruce, N.J. Windsor, Aust. J. Chem. 30 (1977) 1601–1604.

[37] C. Stren, P.J. Carroll, R.K. Kohli, E. Meggers, J. Organomet. Chem. 693 (2008) 551-556.

[38] G.M. Sheldrick, SHELXL-97: An Integrated System for Solving and Refining Crystal Structures from Diffraction Data (Revision 5.1); University of Göttingen, Germany, 1997.

[39] Y. Zhao, D.G. Truhlar, J. Chem. Phys. 125 (2006) 1-18.

[40] Y. Zhao, D.G. Truhlar, Theor. Chem. Acc. 120 (2008) 215-41.

[41] Gaussian 09, Revision B.01, M.J. Frisch, G.W. Trucks, H.B. Schlegel, G.E. Scuseria, M.A. Robb, J.R. Cheeseman, G. Scalmani, V. Barone, B. Mennucci, G.A. Petersson, H. Nakatsuji, M. Caricato, X. Li, H.P. Hratchian, A.F. Izmaylov, J. Bloino, G. Zheng, J.L. Sonnenberg, M. Hada, M. Ehara, K. Toyota, R. Fukuda, J. Hasegawa, M. Ishida, T. Nakajima, Y. Honda, O. Kitao, H. Nakai, T. Vreven, J.A. Jr. Montgomery, J.E. Peralta, F. Ogliaro, M. Bearpark, J.J. Heyd, E. Brothers, K.N. Kudin, V.N. Staroverov, R. Kobayashi, J. Normand, K. Raghavachari, A. Rendell, J.C. Burant, S.S. Iyengar, J. Tomasi, M. Cossi, N. Rega, J.M. Millam, M. Klene, J.E. Knox, J.B. Cross, V. Bakken, C. Adamo, J. Jaramillo, R. Gomperts, R.E. Stratmann, O. Yazyev, A.J. Austin, R. Cammi, C. Pomelli, J.W. Ochterski, R.L. Martin, K. Morokuma, V.G. Zakrzewski, G.A. Voth, P. Salvador, J.J. Dannenberg, S. Dapprich, A.D. Daniels, Ö. Farkas,J.B. Foresman, J.V. Ortiz, J. Cioslowski, D.J. Fox, Gaussian, Inc., Wallingford CT, 2009.

[42] S.S. Leang, F. Zahariev, M.S. Gordon, J. Chem. Phys. 136 (2012) 10410.

[43] P.J. Hay, W.R. Wadt, J. Chem. Phys. 82 (1985) 270-83.

[44] P.J. Hay, W.R. Wadt, J. Chem. Phys. 82 (1985) 299-310.

[45] G. Scalmani, M.J. Frisch, B. Mennucci, J. Tomasi, R. Cammi,V. Barone, *J. Chem. Phys.* 124 (2006) 1-15.

[46] F. Furche, R. Ahlrichs, J. Chem. Phys. 117 (2002) 7433-47.

[47] J. Tomasi, B. Mennucci, R. Cammi, Chem. Rev. 105 (2005) 2999-3093.

[48] A.L.Tenderholt, "QMForge: A Program to Analyze Quantum Chemistry Calculations", Version 2.3.2, http://qmforge.sourceforge.net

[49] http://www.chemcraftprog.com

[50] A. Sanz-Medel, T. Jakusch, D. Hollender, E.A. Enyedy, C.S. Gonzalez, M. Montes-Bayon, J.C. Pessoa, I. Tomaz, T. Kiss, Dalton Trans. (2009) 2428–2437.

[51] B. Demoro, R.F.M. de Almeida, F. Marques, C.P. Matos, L. Otero, J.C. Pessoa, I. Santos, A. Rodríguez, V. Moreno, J. Lorenzo, D. Gambino, A.I. Tomaz, Dalton Trans. 42 (2013) 7131–7146.

[52] A. Coutinho, M. Prieto, M. J. Chem. Educ. 70 (1993) 425–428.

[53] M. Kubista, R. Sjoback, S. Eriksson, B. Albinsson, B. Analyst 119 (1994) 417–419.

[54] B. Valeur, Molecular Fluorescence: Principles and Applications, Wiley-VCH Verlag GmbH, 2001.

[55] T.S. Morais, F.C. Santos, T.F. Jorge, L. Côrte-Real, P.J.A. Madeira, F. Marques; M.P. Robalo, A. Matos, I. Santos, M.H. Garcia, J. Inorg. Biochem. 130 (2014) 1-14.

[56] A. Bergamo, A. Masi, A.F.A. Peacock, A. Habtemariam, P.J. Sadler, G. Sava, J. Inorg. Biochem. 104 (2010) 79–86.

Table 1. Selected DFT structural data and estimated CDA π-backdonations for compounds **1**, **5**-**7**.

Compound	**1**	**5**	**6**	**7**
Bond Distances				
Ru-Cp[a]	1.7879	1.7839	1.8763	1.9039
Ru-N[b]	2.1439	2.1523	2.1484	2.1202
Ru-X[c]	2.1997	2.5423	1.8870	2.4765
Bond Angles				
Cp-Ru-X	127.39	131.12	124.82	125.38
N-Ru-N	74.85	74.77	75.03	76.15
π-bakdonation (in electrons)[d]				
$[CpRu(bipy)]^+ \rightarrow L$	0.405	0.250	0.765	0.546
$[CpRuL]^+ \rightarrow bipy$	0.543	0.658	0.598	0.584

a - Centroid; b - Average Ru-N bonds; c - X= N, S, C or P for compounds **1**, **5**, **6** and **7** respectively; d - calculated by CDA.

Table 2. Experimental and TD-DFT calculated optical data for complex **7** in acetonitrile

Experimental λ_{max} (nm)[a]	Calculated λ_{max} (nm)[a]	Vertical Excitations (nm)	Oscillator Strength (f)	Major Contributions	Attribution
-	580.0	578	0.01	94.9% H-1 → L	(d-π*bipy)
467	470	469.5	0.039	82.9% H-2 → L	(d-π*bipy)
414	405	411.4	0.049	61.6% H → L+3	(d-d*)
		400.4	0.032	63.3% H-1 → L+2 21.1% H → L+4	(d-π*bipy) (d-d*)
353 (sh)	356	364.7	0.029	31.4% H-2 → L+1 23.8% H-1 → L+5	(d-π*bipy) (d-π*phosp)
		352.3	0.011	71.6% H-3 → L	(d-π*bipy)
		350.7	0.033	40.9% H-2 → L+2	(d-d*)
		348.2	0.020	79.3% H-1 → L+6	(d-π*phosp)
290	281	283.0	0.259	25.8% H-7 → L 24.6% H-1 → L+11	π-d* d-π*bipy
		276.1	0.085	65.5% H-3 → L+2	πphosp-π*bipy

a - the presented values refer to the maxima of the convoluted bands; b - H = HOMO, L = LUMO

Table 3. *In vitro* cytotoxic activity of complexes **5**-**7** against A2780 ovarian, MCF7 and MDAMB231 breast adenocarcinoma at 72 h measured as the half-inhibitory concentration (IC_{50}).

Compound	IC_{50} (μM)		
	MCF7	A2780	MDAMB231
5	323 ± 59	238 ± 51	>> 200
6	96.4 ± 49	49 ± 12	205 ± 32
7	5.9 ± 1.8	2.2 ± 0.9	5.8 ± 3.0
Cisplatin	36 ± 8.0[27],*	1.9 ± 0.1[27],*	110 ± 28[28],*

*Obtained with the same experimental conditions.

Table 4. Crystal data and structure refinement for $[Ru(\eta^5\text{-}C_5H_5)(bipy)PPh_3][PF_6]\cdot(CH_3)_2CO$ **7**.

Formula	$C_{36}H_{34}F_6N_2OP_2Ru$
Formula weight	787.66
T, *K*	100(2)
Wavelength, Å	0.71073
Crystal system	Monoclinic
Space group	C2/c
a/Å	36.6872(10)
b/Å	11.0435(3)
c/Å	18.0857(5)
β/º	113.136(2)
V/Å^3	6738.2(3)
Z	8
F_{000}	3200
D_{calc}/g cm^{-3}	1.553
μ/mm^{-1}	0.626
θ/ (º)	1.21 to 30.69
R_{int}	0.0523
Crystal size/ mm^3	0.50 x 0.45 x 0.42
Goodness-of-fit on F^2	1.125
R_1 [a]	0.0305
wR_2 (all data) [b]	0.1002
Largest differences peak and hole (eÅ^{-3})	0.986 and -0.783

[a] $R_1 = \Sigma \| |F_o| - |F_c| \| / \Sigma |F_o|$. [b] $wR_2 = \{\Sigma[w(|F_o|^2 - |F_c|^2)^2] / \Sigma[w(F_o^4)]\}^{1/2}$

Figure/Schemes captions

Scheme 1. Reaction scheme for the synthesis of the new $[Ru(\eta^5\text{-}C_5H_5)(bipyridine)(L)][PF_6]$ complexes and the structures of the ligands numbered for NMR assignments. *Compound **7** was obtained following a different synthetic route (see experimental section)

Figure 1. UV−visible spectrum for a) complex **1** in acetonitrile, typifying the general behaviour of complexes **1**-**7**; b) comparison of UV-Vis spectra of compounds **1** (──), **5** (- - -), **6** (─ ─ ─) and **7** (·····) showing the shift of MLCT bands.

Figure 2. ORTEP plot for the cation complex $[Ru(\eta^5\text{-}C_5H_5)(bipy)PPh_3]^+$ **7**. All non-hydrogen atoms are presented by their 30% probability ellipsoids. Hydrogen atoms are omitted for clarity.

Figure 3. Cyclic voltammogram of complex **3** in dichloromethane (solid line), showing the isolated Ru(II)/Ru(III) process (dashed line) (0.2 M tetrabutylammonium hexafluorophosphate, scan rate: 200 $mV.s^{-1}$).

Figure 4. Cyclic voltammograms for complexes **1** (solid line) and **8** (dashed line) in acetonitrile (0.1 M tetrabutylammonium hexafluorophosphate, scan rate: 200 $mV.s^{-1}$).

Figure 5. Trend of the oxidation potentials (E_{pa}) for the series of complexes $[RuCp(bipy)(L)][PF_6]$ in acetonitrile solution.

Figure 6. Experimental (·····) and calculated (──) spectra for complex **7** in acetonitrile solution. The TD-DFT intensity was normalized for a better illustration.

Figure 7. Effect of complex **5** on HSA fluorescence emission. a) Emission spectra of HSA (λ_{exc} = 295 nm) in the absence (red circles with the highest absorbance, 310-510 nm) and in the presence (black lines) of increasing concentrations of Ru-complex in 2% DMSO/10 mM HEPES pH 7.4; b) % Relative intensity plots (IFE corrected data) obtained at 340 nm for complex **5** (rhombus), **6** (triangles) and **7** (squares).

Figure 8. Effect of HSA on the cytotoxicity of complexes **5** and **6** on MCF7 cells after a 72 h challenge. MCF7 cells were treated with complex **5** and **6** at 320 and 200 μM, respectively, and pre-incubated with HSA at 1:0.5 complex-to-protein molar ratio. Data labels shown are the mean values (±SD) of two independent experiments, each performed with at least six replicates. Control indicates cells with no treatment (negative control); HSA 160 or 100 μM indicate cells treated with HSA alone, **5** 320 μM and **6** 200 μM are cells treated with the complexes in the absence of albumin.

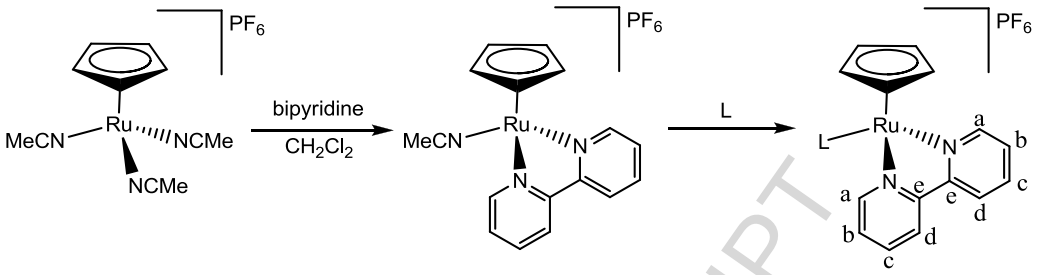

L =

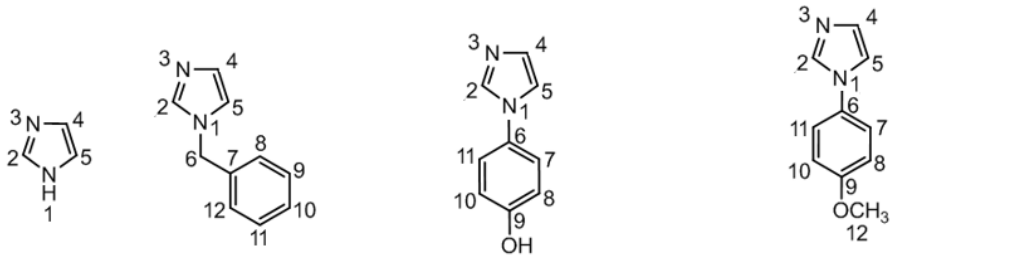

imidazole **1**

1-benzyl-1*H*-imidazole **2**

4-(1*H*-imidazol-1-yl)phenol **3**

1-(4-methoxyphenyl)-1H-imidazole **4**

dimethylsulfoxide **5**

carbon monoxide **6**

triphenylphosphane **7***

acetonitrile **8**

Scheme 1.

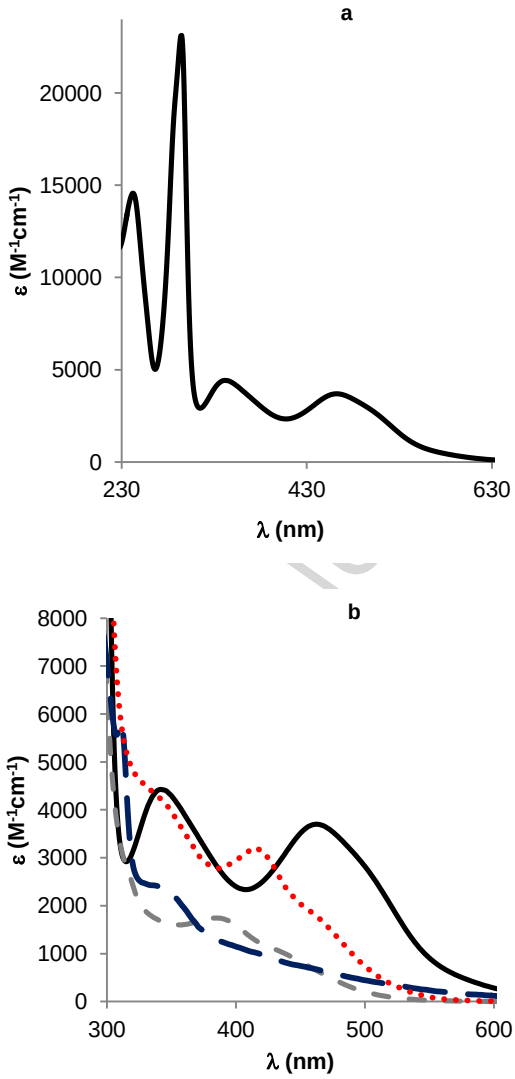

Figure 1.

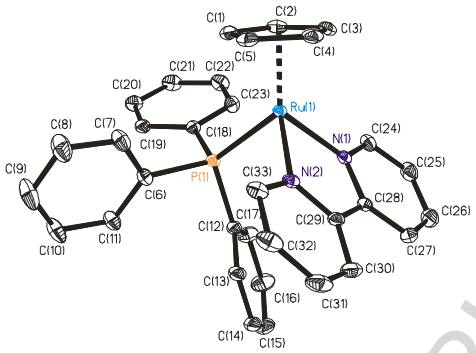

Figure 2.

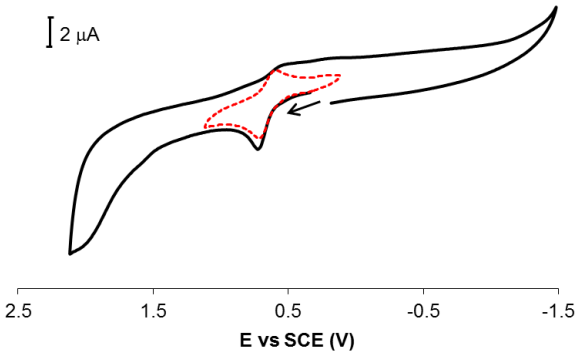

Figure 3.

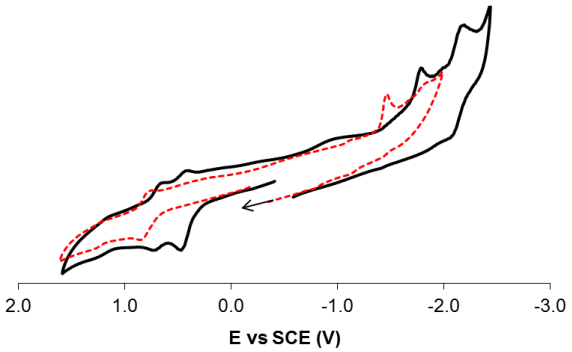

Figure 4.

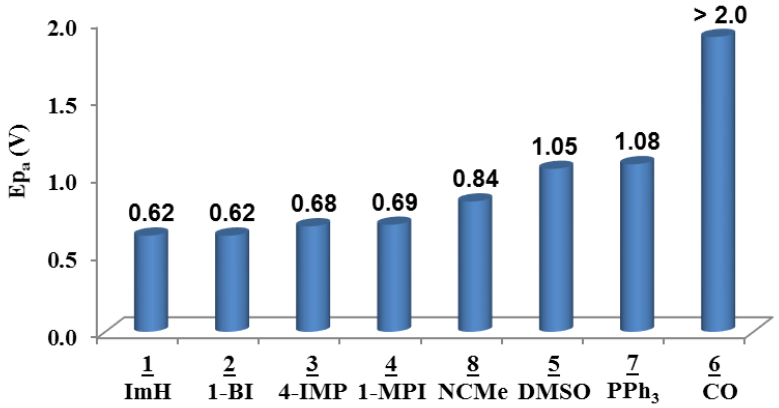

Figure 5.

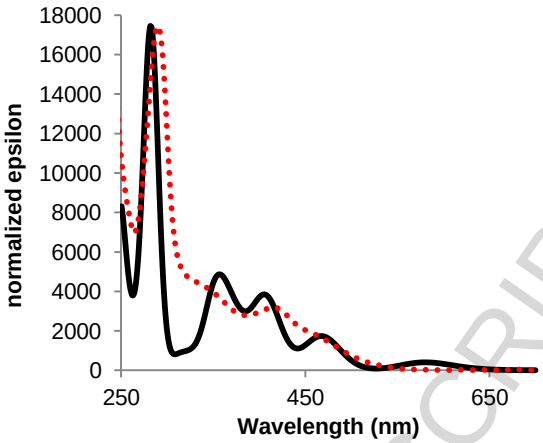

Figure 6.

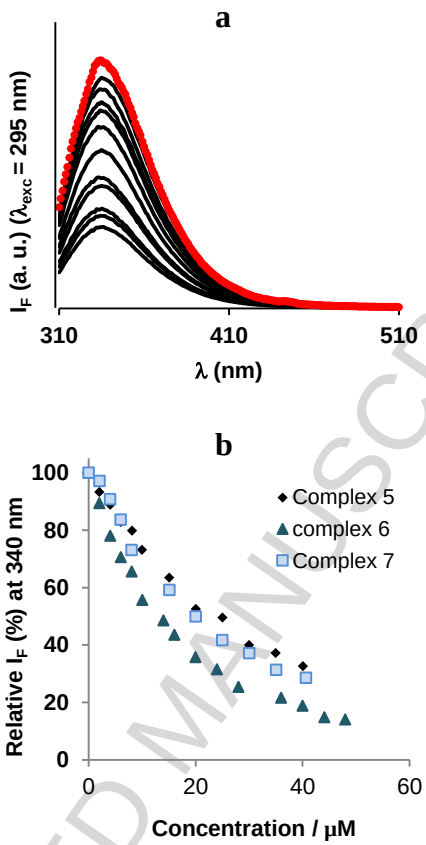

Figure 7.

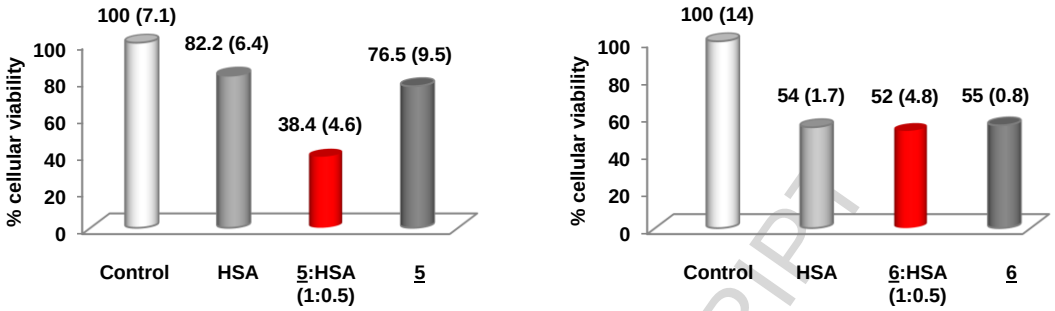

Figure 8.

Graphical Abstract

New family of [Ru(η^5-C_5H_5)(bipyridine)(L)][PF_6] complexes shows that 'L' plays an important role in electronic activation of the bipyridine. The best cytotoxic effect was observed for the best electronic activation of this ligand.

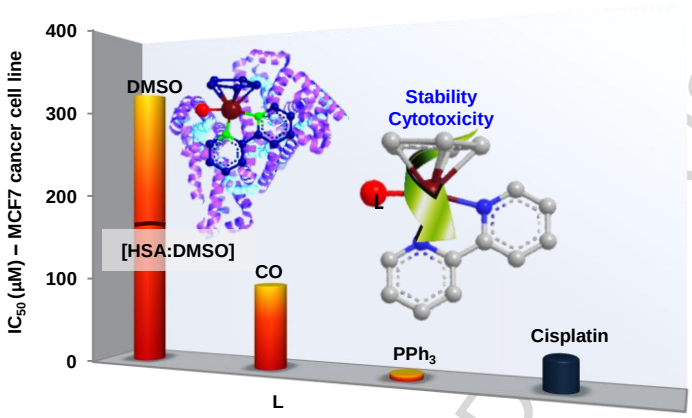

Highlights

- New family of [Ru(η^5-C_5H_5)(bipyridine)(L)][PF_6] complexes
- Structure-activity correlations drawn by spectroscopic, electrochemical and DFT data
- 'L' has a crucial role in the fine-tuning of the electronic density at Ru centre
- Best cytotoxic effect in human cancer cells found for the best electronic activation of bipyridine